Ferroelectric and dielectric properties of BF-PT/LNO thin films on different substrates

Hao Wang[1], Jian Zhai[1], Wenhui Lu[1], Jianguo Chen[1], and Jinrong Cheng[1,*]

[1] School of Materials Science and Engineering, Shanghai University, 333 Nanchen Road, Shanghai 200444, China

Received: 2 August 2020
Accepted: 9 December 2020
Published online:
11 January 2021

© The Author(s), under exclusive licence to Springer Science+Business Media, LLC part of Springer Nature 2021

ABSTRACT

Ferroelectric $0.7BiFeO_3$–$0.3PbTiO_3$ (BF-PT) thin films were prepared by the sol–gel method on $Pt/Ti/SiO_2/Si$, stainless steel (SS) and Ti substrates, respectively, with $LaNiO_3$ (LNO) buffer layers. The performance of the BF-PT films on SS is significantly better than that on the Ti substrates and is comparable to the films on the $Pt/Ti/SiO_2/Si$ substrates. The BF-PT films on SS substrates have the good crystallinity with a pure perovskite structure. Moreover, the dielectric loss and remnant polarization (P_r) of BF-PT on SS are of 4.48% (at the frequency of 10^3 Hz) and 28.9 μC/cm^2, respectively, revealing good dielectric and ferroelectric properties. It is found that BF-PT deposited on SS has the good fatigue resistance relative to the films on Ti substrates. The reduction of polarization is of about 22% after the electrical switching of 1.33×10^8 cycles. Experiments show that BF-PT thin films deposited on SS substrates exhibit superior ferroelectric, dielectric, and fatigue resistance properties.

1 Introduction

The xBiFeO$_3$–(1−x)PbTiO$_3$ (BF-PT) solid solutions attracted a lot of attention from scientists and engineers during the past few decades, because their c/a ratios above 1.18 and the Curie temperature over 623 °C can be obtained near the morphotropic phase boundary (MPB) of $x \approx 0.7$ [1]. The solid solutions exhibit pure tetragonal structure for $x \leq 0.69$, rhombohedral structure for $x \geq 0.73$, and two phase for $0.69 < x < 0.73$ (rhombohedral and tetragonal); the tetragonality of the BF-PT solid solutions is 6–19%, which is more than that of pure lead titanate [2, 3]. Additionally, BF-PT solid solutions can exhibit excellent ferroelectric and ferromagnetic properties [4, 5]. Thus, BF-PT ceramics have good application prospects for high-temperature piezoelectric devices, electromechanical transducers, and high-power solid-state transformers [6, 7]. Thin films have advantages over bulk ceramic materials such as miniaturization, which have potential applications in microelectronic mechanical intelligent devices such as ferroelectric memories and capacitors [8, 9]. Previous studies have shown that doping can be used to improve the performance of ferroelectric materials. For example, the ferromagnetic and ferroelectric properties of $Bi_{0.95}Dy_{0.05}Fe_{0.95}M_{0.05}O_3$ (M = Mn, Co) ceramics prepared by the co-doping of Dy–Mn and

Address correspondence to E-mail: jrcheng@staff.shu.edu.cn

https://doi.org/10.1007/s10854-020-05081-0

Dy–Co with $BiFeO_3$ (BF) ceramics have been improved. For ferroelectric thin films, the microstructure and electrical properties strongly depend on the characteristics of the underlying substrates [10]. For example, the BF thin films deposited on $NdGaO_3$ (NGO) and $SrTiO_3$ (STO) substrates showed structures with just 109° domain walls as well as with 71° and 109° domain walls, respectively [11]. The BF thin films on STO have a diamond-shaped structure, while the BF films on $LaAlO_3$ (LNO) possess tetragonal lattice [12]. Compared with conventional Si substrates, ferroelectric thin films deposited on base metals are better for their integration with engineering systems [13, 14]. Additionally, these low-cost metal substrates can act as both the bottom electrode and the substrates to avoid the complicated micro-machining of the silicon substrates [15, 16] and to simplify the overall device manufacturing. In our previous work, we studied the ferroelectric and dielectric properties of $Pb(Zr_{0.53}Ti_{0.47})O_3$ (PZT) ferroelectric films deposited on SS and Ti substrates, as well as La-doped BF-PT films deposited on Pt-covered Si wafers [17–19]. The presence of the LNO buffer layers can improve the ferroelectric performance of BF-PT thin films [20]. Recently, the ferroelectric $Na_{0.5}Bi_{0.5}(Ti_{0.98}Fe_{0.02})O_3$ (NBTFe) thin films and the perovskite structure Nd_2NiMnO_6 (NNMO) thin films deposited on different substrates were reported in the literature [21, 22]. However, under the same preparation conditions, analysis of BF-PT thin films properties as a function of the various underlying substrates was rarely reported. Therefore, this work demonstrates the BF-PT thin films deposition on $Pt/Ti/SiO_2/Si$, SS, and Ti substrates with LNO buffer layers. We studied morphology, dielectric, and ferroelectric properties of the resulting films as a function of their underlying substrates. The effects of substrates on the leakage current and fatigue performance of BF-PT films were also analyzed.

2 Experimental

0.1 mol/L LNO precursor and 0.4 mol/L BF-PT sols were prepared using $Bi(NO_3)_3{\cdot}5H_2O$, $Fe(NO_3)_3{\cdot}9H_2O$, $Pb(CH_3COO)_2$, $Ti(OC_3H_9)_4$, and 2-methoxyethanol (2-MOE). An additional 10 at% of Pb was added to account for the Pb loss during the solution preparation and heating at 90 °C for 2 h. The resulting solution was 0.4 mol/L $0.7BiFeO_3$–$0.3PbTiO_3$ (BF-PT) sol.

LNO sol was spin-coated on SS, Ti, and $Pt/Ti/SiO_2/Si$ substrates at 3500 rpm. Each layer was heated in the O_2 atmosphere for 5 min at 550 °C. This stage was repeated until the desired film thickness was obtained. 150 nm thick LNO layer was obtained by 15 min annealing in the air at 700 °C. BF-PT sol was deposited at 3500 rpm on SS, Ti, and $Pt/Ti/SiO_2/Si$ substrates containing LNO buffer layer. Each layer was heated for 5 min in pure O_2 at 500 °C. This stage was repeated eight times. Finally, a 0.4 mm Au layer, acting as an electrode, was deposited on BF-PT films through a shadow mask.

The phase structure of the films was obtained by X-ray diffraction (XRD) performed using the DLMAX-2550 instrument. Film morphologies were analyzed by scanning electron microscopy (SEM) performed using a JEOL JSM7000F instrument. The leakage current, as well as dielectric and ferroelectric properties, was analyzed by Agilent 4294A impedance analyzer and Precision Premier II ferroelectric tester.

3 Results and discussion

3.1 Phase structure and surface morphology

XRD of BF-PT thin films on different substrates showed patterns corresponding to the perovskite structure (see Fig. 1). The intensity of the (110) peak was in the following order: SS > $Pt/Ti/SiO_2/Si$ > Ti. Thus, the films deposited on SS and $Pt/Ti/SiO_2/Si$ had higher crystallization degree. XRD peaks belonging to metallic Cr and Fe were observed for the samples deposited on the SS substrates because it contained ~ 19% of Cr and a lot of Fe. (110) TiO_2 peak observed in the XRD patterns of the samples deposited on the Ti substrates was due to the Ti oxidation and diffusion during annealing in the oxygen atmosphere. Above 500 °C, Ti is mainly oxidized to Ti^{4+} and the oxidation products of TiO_2 > Ti_2O_3 > TiO under sufficient O_2 atmosphere [23], so the results show that Ti element diffuses. The main oxidation product is TiO_2, and the degree of diffusion at the bottom is much larger than that of the SS substrates.

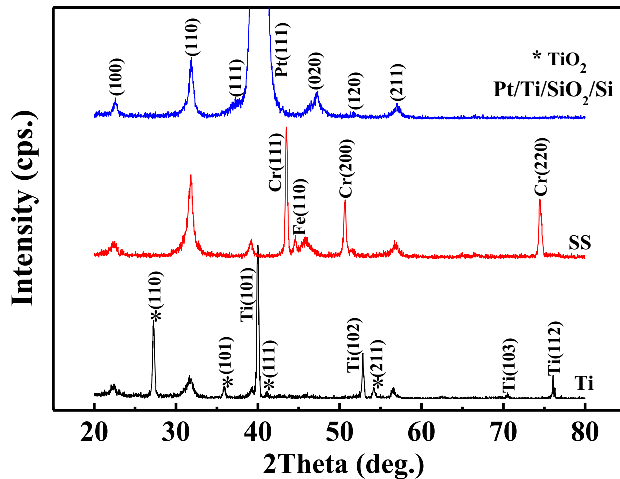

Fig. 1 XRD patterns of BF-PT thin films for different substrates

SEM of BF-PT films on SS and $Pt/Ti/SiO_2/Si$ were more uniform with denser structure and larger average grain size (~ 50 nm) than the films deposited on Ti substrates (see Fig. 2), which had rougher morphology and only some pores. Additionally, crystal grain sizes of films deposited on the Ti substrates were not uniform, mostly because of the inhomogeneous Ti substrate texture formed during annealing [24]. This initial substrate surface roughness had a great impact on the thin films grain development during the early nucleation stages.

The cell parameters of BF-PT films, Ti, SS, and $Pt/Ti/SiO_2/Si$ substrates were 3.7957 Å, 4.6843 Å, 3.599 Å, and 4.6843 Å, respectively. According to the lattice mismatch formula, $\delta = \frac{2|a_s - a_e|}{a_s + a_e}$, where δ is lattice mismatch, α_s is the cell parameter of the substrate, *and* α_e is cell parameter of the thin films, we can get the lattice mismatch of three substrates: Ti > SS > $Pt/Ti/SiO_2/Si$. The thermal expansion coefficients of Ti and SS substrates were 10.8×10^{-6}/k and 14×10^{-6}/k, respectively. Therefore, the thermal expansion of SS substrates is more obvious at high temperature, so LNO buffer layer is added to reduce the influence of substrates on the thin films. According to the Raman diffraction pattern (see Fig. 3), it can be seen that the width of the Raman peak of $Pt/Ti/SiO_2/Si$ substrates becomes narrower and the peak is also relatively sharp. To sum up, we speculated that the stress on $Pt/Ti/SiO_2/Si$ substrates was minimum, and the total stress on Ti was greater than that on SS substrates.

3.2 Electrical properties

We analyzed the relationship between the dielectric constant (ε_r) and the dielectric constant loss (tanδ) of BF-PT thin films deposited on different substrates. In addition to the dielectric relaxation of BF-PT films

Fig. 2 SEM images of BF-PT thin films prepared on different substrates: **a** Ti, **b** SS, and **c** $Pt/Ti/SiO_2/Si$

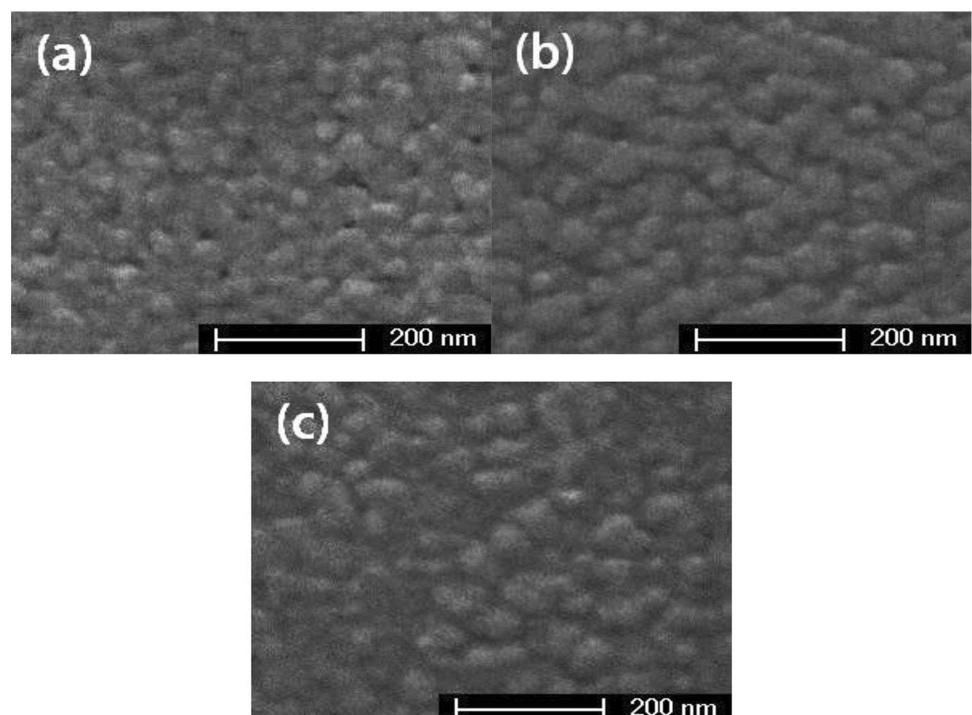

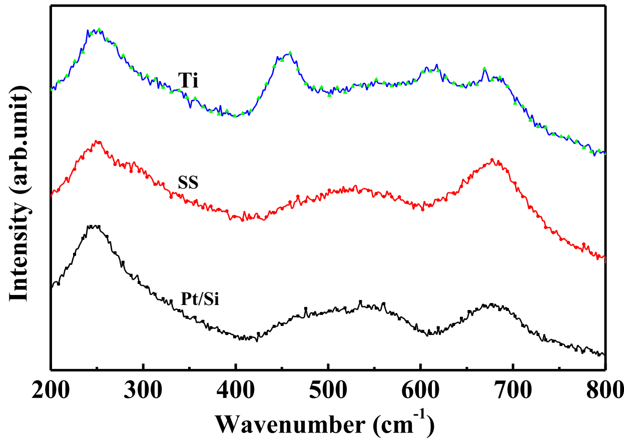

Fig. 3 Raman spectra on different substrates

deposited on SS at high frequencies, the dielectric constant of films on SS was higher than that of the films deposited on Ti substrates at 10^3–10^5 Hz (reaching 483.0 at 10^3 Hz, see Fig. 4a). The dielectric loss of BF-PT films deposited on Pt/Ti/SiO_2/Si and SS gradually increased with frequency. However, the dielectric loss of the films on Ti substrates (which was equal to 11.7% at 10^3 Hz) decreased as the frequency increased. This value was much higher than the dielectric losses obtained for the films deposited on Pt/Ti/SiO_2/Si and SS (which were equal to 4.1% and 4.5%, respectively).

Analysis of the hysteresis loops at 600 kV/cm showed that the remnant polarization (P_r) values of the BF-PT films deposited on Pt/Ti/SiO_2/Si, SS, and Ti substrates were equal to 34.8, 28.9, and 25.0 μC/cm^2, respectively. Corresponding coercive field (E_c) values were equal to 141.6, 184.9, and 227.9 kV/cm, respectively (see Fig. 4b).

The ferroelectric performance of BF-PT films deposited on SS were similar to the films deposited on Pt/Ti/SiO_2/Si, but higher than that of the films deposited on Ti. The diffusion and oxidation of metal ions in thin films deposited on metallic substrates were the major factors causing the dielectric and ferroelectric properties of ferroelectric films to deteriorate. XRD showed that Ti substrates underwent more severe oxidation and diffusion deformations than the SS substrates. The diffusion of Ti^{4+} ions, formed during the substrate oxidation, very likely formed an internal electric field forcing the anions to move in the direction opposite to the applied electric field. Ti^{4+} presence in the substrate ions very likely increased the number of defects, which, in turn, increased the coercive field and decreased polarization of corresponding deposited films [25]. The roughness of the oxidized Ti affected the LNO buffer layer bonding and crystallization, as well as increased its conductivity, all of which caused the lattice mismatch between LNO and BF-PT. All these factors explain the poor ferroelectric properties of the BF-PT films deposited on Ti.

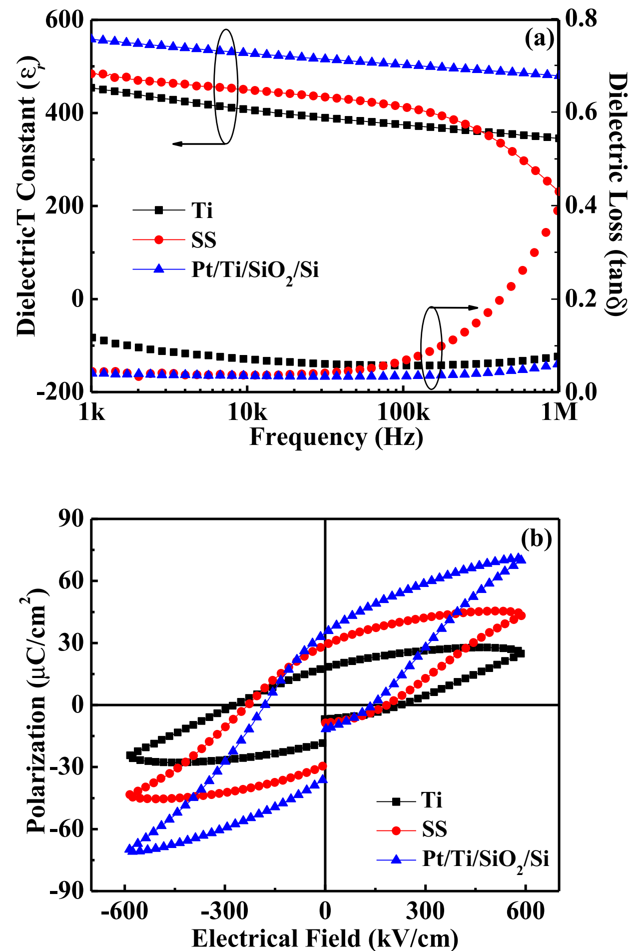

Fig. 4 **a** Dielectric constant ε_r and loss tanδ as a function of frequency of the BF-PT thin films for different substrates, **b** *P*–*E* loop of the BF-PT thin films for different substrates

The leakage current density of BF-PT films deposited on Ti was 1–1.5 order of magnitude higher than that of the films deposited on SS substrates (see Fig. 5a). As the voltage of the electric field was increased, the leakage current density of the films on SS substrates tends to be moderate. Leakage current density of the films deposited on Ti increased above 200 kV/cm rapidly by two orders of magnitude.

The ln*J*–ln*E* diagram of the leakage current density (*J*) and the applied field strength (*E*) showed linear

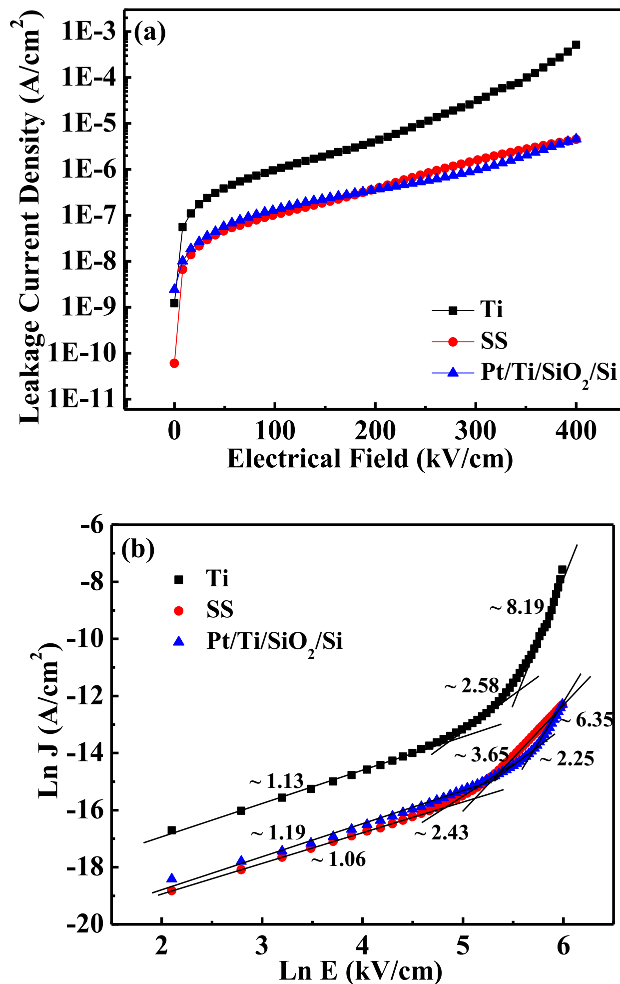

Fig. 5 **a** Leakage current density of the BF-PT thin films for different substrates, **b** lgJ-lgE curves of the BF-PT thin films for different substrates

ln$J$–ln$E$ curves in low field strength region for the BF-PT films deposited on Ti, SS, and Pt/Ti/SiO_2/Si with the corresponding slopes equal to 1.13, 1.06, and 1.19, respectively (see Fig. 5b). Such behavior is indicative of a leakage current mechanism based on ohmic conduction [26, 27]. In the mid field strength region, an internal electric field is formed after the defects capture the free carriers. The injected carriers form a space charge accumulation region inside the BF-PT films. As a result, the slopes of the corresponding ln$J$–ln$E$ curves changed to 2.58, 2.43, and 2.25. Thus, the leakage conductance mechanism, in this case, was based on the space charge limiting current (SCLC). In the high field strength region, the slopes increased to 8.19, 3.65, and 6.35. At the same time, the leakage current on SS substrates was still based on the SCLC. The leakage current and electric field of the films deposited on Ti and Pt/Ti/SiO_2/Si substrates showed a high exponential change relationship, indicating that the defect impurity traps gradually became filled with carriers, which reduced the effective empty trap density and increased the effective electron mobility. In this situation, the leakage current mechanism was based on a trap charge limitation current (TCLC).

3.3 Fatigue and retention

Analysis of the normalized polarization as a function of electrical switching cycles showed that BF-PT films deposited on Pt/Ti/SiO_2/Si possessed the best fatigue resistance. The fatigue resistance of the films deposited on the SS was better than that of the films deposited on Ti (see Fig. 6a). When the electrical switching cycles were increased from 1.33×10^7 to 1.33×10^8, the normalized polarization of BF-PT films deposited on SS decreased from 86.9 to 78.7%. Similar values for the films deposited on Ti substrates decreased from 84.2 to 62.7%.

The normalized polarization of BF-PT films deposited on the Ti substrates decreased as the retention time (in the 1–10^4 s range) increased (see Fig. 6b), which indicates poor performance. However, the normalized P_r of the films deposited on SS substrates was close to the values observed for the films deposited on Pt/Ti/SiO_2/Si: almost no change was observed during the 300 s retention time. At 10^4 s retention time, the reduction values of polarization of BF-PT films deposited on Ti, SS, and Pt/Ti/SiO_2/Si substrates were equal to 19.5%, 13.6%, and 9.6%, respectively.

The worst fatigue and retention values were observed for the films deposited on Ti substrates, which agrees with the trends observed for other dielectric and ferroelectric property trends. The film fatigue and retention performance are strongly related to the defective dipoles that cause aging. The internal bias field generated by the defective dipoles can reverse the flipped domains over time and degrade the polarization as a function of time and the number of switching cycles. Oxygen vacancy defects are more likely to form during the crystallization process, which, in turn, might negatively affect the fatigue and retention resistance [28, 29]. The effect of the diffusion and oxidation of elements in the films deposited on Ti substrates is more serious than for the films of the SS substrates. Thus, thin films on Ti

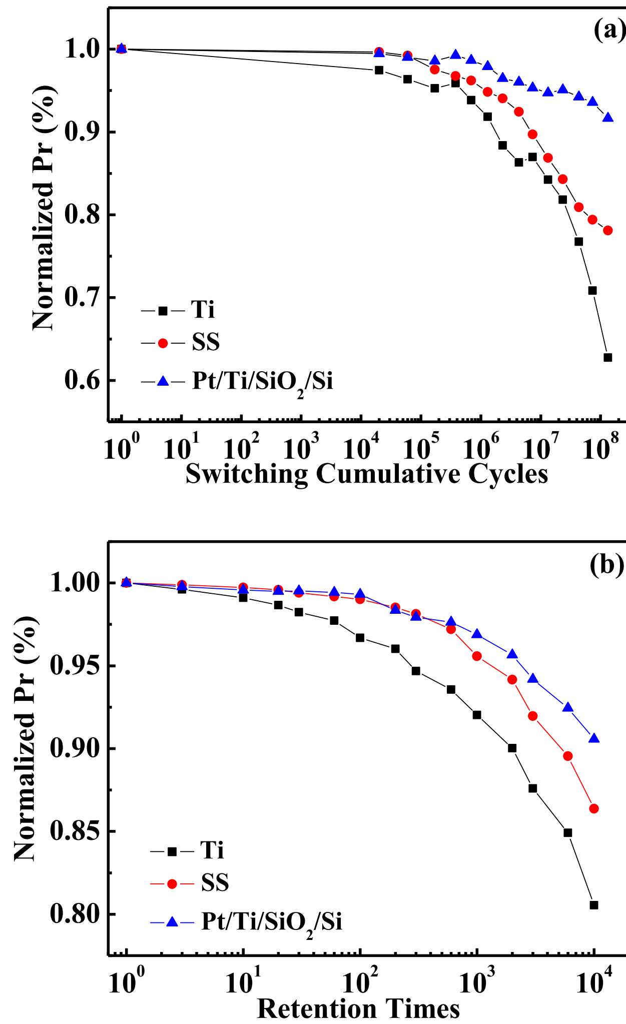

Fig. 6 **a** Fatigue characteristics of BF-PT thin films for different substrates, **b** Retention behaviors of BF-PT thin films for different substrates

typically have higher numbers of cation and anion defects and, as a result, poor fatigue and retention performance.

4 Conclusions

BF-PT thin films with LNO buffer layers were prepared on SS, Ti, and $Pt/Ti/SiO_2/Si$ substrates by the sol–gel method. The dielectric and ferroelectric properties of BF-PT on SS substrates are comparable with that of the films on $Pt/Ti/SiO_2/Si$ substrates and much greater than that of the films on Ti substrates. BF-PT films on SS reveal the superior fatigue and retention resistance to that of the films on Ti substrates. TiO_2 diffraction peaks were observed on Ti substrates, indicating that the oxidation and diffusion of Ti elements were quite intense, resulting in the deterioration of the electrical properties of BF-PT thin films.

Acknowledgements

This work was supported by the National Natural Science Foundation of China (Grant Nos. 51672169, 51872180 and 51302163) and Natural Science Foundation of Shanghai (Grant No. 18ZR1414800).

References

1. V.V.S.S.S. Sunder, A. Halliyal, A.M. Umarji, J. Mater. Res. **10**, 1301 (1995)
2. R. Ranjan, K.A. Raju, Phys. Rev. B **82**, 54119 (2010)
3. S. Bhattacharjee, S. Tripathi, D. Pandey, Appl. Phys. Lett. **91**, 042903 (2007)
4. M.A. Khan, T.P. Comyn, A.J. Bell, Appl. Phys. Lett. **91**, 32901 (2007)
5. S. Gupta, A. Garg, D.C. Agrawal, S. Bhattacharjee, D. Pandey, J. Appl. Phys. **105**, 14101 (2009)
6. W.M. Zhu, Z.G. Ye, Ceram. Int. **30**, 1435 (2004)
7. S. Dong, J.F. Li, D. Viehland, J. Mater. Sci. **41**, 97 (2006)
8. H. Li, J. Zhu, J. Zhuang, Y. Hu, M. Huai, Q. Yang, J. Sol-Gel, Sci. Technol. **75**, 353 (2015)
9. W. Sakamoto, A. Iwata, T. Yogo, J. Appl. Phys. **104**, 104106 (2008)
10. W. Zhang, X. Zhu, L. Wang, X. Xu, Q. Yao, W. Mao, X. Li, J. Supercond. Nov. Magn. **30**, 11 (2017)
11. H.X. Lu, J.L. Zhao, J.R. Sun, J. Wang, B.G. Shen, Phys. B **406**, 305 (2011)
12. Z. Chen, X. Zou, W. Ren, L. You, C. Huang, Y. Yang, L. Bellaiche, Phys. Rev. B **86**, 235125 (2012)
13. R. Bouregba, G. Poullain, B. Vilquin, H. Murray, Mater. Res. Bull. **35**, 1381 (2000)
14. M. Okada, K. Tominaga, T. Araki, S. Katayama, Y. Sakashita, Jpn. J. Appl. Phys. **29**, 718 (1990)
15. S. Huang, J. Chen, J. Cheng, J. Sol-Gel, Sci. Technol. **73**, 278 (2015)
16. H. Dong, G. Lu, D. Chen, D. Jin, J. Chen, J. Cheng, J. Sol-Gel, Sci. Technol. **80**, 848 (2016)
17. H. Li, S. Wang, J. Jian, H. Dong, J. Chen, D. Jin, J. Cheng, J. Mater. Sci.-Mater. Electron. **29**, 14651 (2018)
18. H. Dong, J. Jian, H. Li, D. Jin, J. Chen, J. Cheng, J. Alloys Compd. **725**, 54 (2017)
19. D. Chen, S. Huang, J. Chen, J. Cheng, J. Sol-Gel, Sci. Technol. **76**, 220 (2015)

20. S. Wang, H. Wang, J. Jian, J. Chen, J. Cheng, J. Alloys Compd. **784**, 231 (2019)
21. Q. Yao, C. Yang, F. Geng, C. Feng, P. Lv, X. Zhang, J. Qian, J. Mater. Sci.-Mater. Electron. **27**, 776 (2016)
22. G. Singh, P. Singh, R.J. Choudhary, A. Dogra, J. Alloys Compd. **739**, 586 (2018)
23. G. Lu, S.L. Bernasek, J. Schwartz, Surf. Sci. **458**, 80 (2000)
24. K. Wang, K. Yao, S.J. Chua, J. Appl. Phys. **98**, 13538 (2005)
25. S. Saremi, R. Xu, F.I. Allen, J. Maher, J.C. Agar, R. Gao, L.W. Martin, Phys. Rev. Mater. **2**, 84414 (2018)
26. R. Li, S. Jiang, L. Gao, Y. Li, J. Appl. Phys. **112**, 74113 (2012)
27. S.Y. Wang, B.L. Cheng, C. Wang, S.A.T. Redfern, S.Y. Dai, K.J. Jin, G.Z. Yang, J. Phys. D Appl. Phys. **38**, 2253 (2005)
28. X.J. Meng, J.L. Sun, J. Yu, G.S. Wang, S.L. Guo, J.H. Chu, Appl. Phys. A **73**, 323 (2001)
29. M. Narayanan, B. Ma, U. Balachandran, W. Li, J. Appl. Phys. **107**, 24103 (2010)

Publisher's Note Springer Nature remains neutral with regard to jurisdictional claims in published maps and institutional affiliations.